Volume 57
Number 9
28 January 2021
Pages 1057–1166

# ChemComm

Chemical Communications

rsc.li/chemcomm

ISSN 1359-7345

ROYAL SOCIETY OF CHEMISTRY

**COMMUNICATION**

Jian Li, Lehui Xiao, Zhan-Ting Li, Jun-Li Hou *et al.*
Gramicidin A-based unimolecular channel: cancer cell-targeting behavior and ion transport-induced apoptosis

ChemComm

COMMUNICATION

View Article Online
View Journal | View Issue





Cite this: *Chem. Commun.*, 2021, **57**, 1097

Received 12th December 2020,
Accepted 5th January 2021

DOI: 10.1039/d0cc08073j

rsc.li/chemcomm

# Gramicidin A-based unimolecular channel: cancer cell-targeting behavior and ion transport-induced apoptosis†

Wei-Wei Haoyang,[a] Qi Xiao,[a] Zhongju Ye,[b] Yonghong Fu,[a] Dan-Wei Zhang,[a] Jian Li,*[c] Lehui Xiao,*[b] Zhan-Ting Li*[a] and Jun-Li Hou*[a]

**A series of glycoside–peptide conjugates were prepared by engineering at the N-terminus of the natural peptide gramicidin A. The conjugate containing galactose moiety formed a unimolecular transmembrane channel and mediated ion transport to induce apoptosis of cancer cells. More importantly, it exhibited liver cancer cell-targeting behavior due to the galactose–asialoglycoprotein receptor recognition.**

Gramicidin A (gA) is a linear pentadecapeptide first extracted from soil bacillus in 1939.[1] The peptide consists of alternately arranged L- and D-configurations of amino acids with an N-terminal formyl group, which induces a helical conformation. The peptide can efficiently incorporate into cell membranes to form head-to-head dimerized supramolecular transmembrane channels.[2] This peptide exhibits high antimicrobial activity toward Gram-positive bacteria,[3] which is a result of its ability to mediate ion transport leading to disturbed ion homeostasis of cells.[4] Nevertheless, it shows high hemolysis toxicity, which prevents its further therapeutic applications.[5] gA has also been used as a platform for the construction of artificial channels and molecular devices,[6] and for the investigation of dynamic properties of peptides' interaction with lipid bilayers.[7] Recently, gA was found to exhibit the ability to inhibit cancer cell growth.[8] However, it showed cytotoxicity to healthy cells because of the lack of selectivity for cancer cells over healthy cells.[8c] Herein, we report that by engineering gA with the galactose (Gal) moiety at its N-terminus, the new Gal–gA conjugate was able to target the membrane of liver cancer cells. We have revealed that the conjugate kills the cancer cells through the formation of unimolecular transmembrane channels to mediate ion transport and to disturb the ion homeostasis of the cells.

The asialoglycoprotein receptor (ASGPR) is a lectin predominantly expressed at the liver cell surface and exhibits high affinity for galactose (Gal) and substrates with the Gal moiety.[9] This unique binding feature has been used to develop anticancer drugs targeting liver cancer cells.[10] It has been established that the formyl group at the N-terminus is essential for the formation of head-to-head channels due to its ability to induce the formation of intramolecular hydrogen bonding.[11] The deformylated gA can also form a new channel with a double-stranded helix structure.[12] We envisioned that, by connecting Gal to the N-terminus of the peptide, the conjugate would target liver cancer cells induced by the Gal-ASGPR recognition, thereby mediating ion transport and disturbing ion homeostasis leading to the death of the cells (Fig. 1a).[13] Thus, Gal–gA conjugates **1** and **2** with different spacer lengths have been designed and synthesized (Fig. 1b and Section S2 in the ESI†). To investigate the galactose moiety's influence on targeting, the conjugate **3** containing glucose (Glu), an epimer of galactose, has also been synthesized as a control compound.

Conductance measurements with planar lipid bilayers showed that, in the presence of **1**, ions can flux across the bilayers as indicated by regular square-like signals in the conductance traces (Section S3 in the ESI,† and Fig. 2a). This observation clearly indicates the formation of transmembrane channels in the bilayers.[14] The conductance ($\gamma$) and dwell time ($\tau_{1/2}$) of **1** were determined to be 17.1 ± 2.1 pS and 0.7 ± 0.08 s, respectively (Fig. S10a, ESI†), differing significantly from those of gA (23.0 ± 1.6 pS, 0.4 ± 0.04 s) (Fig. S10b, ESI†). The differences in $\gamma$ and $\tau_{1/2}$ of **1** and gA demonstrated their different channel structures. The fact that **1** exhibited a higher $\tau_{1/2}$ value than gA suggested its higher channel structural stability. Further whole-cell patch clamp experiments showed that the addition of **1** to the patched HepG2 cell solution caused a significant alteration of currents across the cell membrane (Fig. 2b and Section S4 in the ESI†), indicating the incorporation of the molecules into the membrane and the subsequent formation of transmembrane ion channels.

[a] *Department of Chemistry, Fudan University, 220 Handan Road, Shanghai 200433, China. E-mail: houjl@fudan.edu.cn*
[b] *State Key Laboratory of Medicinal Chemical Biology, Tianjin Key Laboratory of Biosensing and Molecular Recognition, College of Chemistry Nankai University, China. E-mail: lehuixiao@nankai.edu.cn*
[c] *Clinical Laboratory Center, Children's Hospital of Fudan University, No. 399 Wanyuan Road, Shanghai 201102, China. E-mail: lijianjulia@fudan.edu.cn*

† Electronic supplementary information (ESI) available. See DOI: 10.1039/d0cc08073j

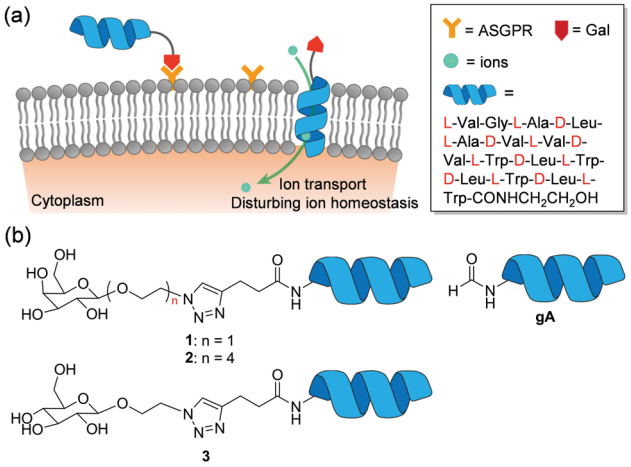


Fig. 1 (a) Schematic presentation of the Gal-ASGPR recognition-mediated targeting behaviour of the channels and ion transport-induced disturbing of ion homeostasis of the cytoplasm. (b) Chemical structures of glycoside–gA conjugates **1–3**.

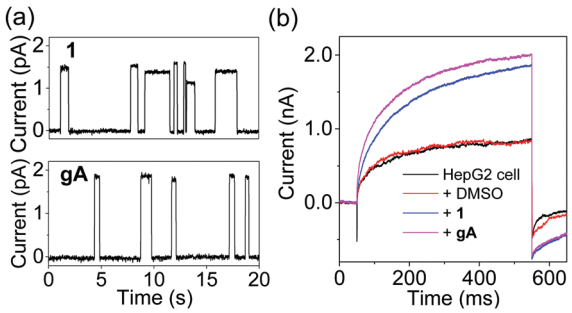


Fig. 2 (a) Single-channel conductance traces of **1** (600 pM) and gA (10 pM) in planar lipid bilayers under +80 mV potential. (b) Whole-cell patch clamp traces of the HepG2 cell in the presence of **1** and gA (1.0 μM) with +40 mV holding voltage.

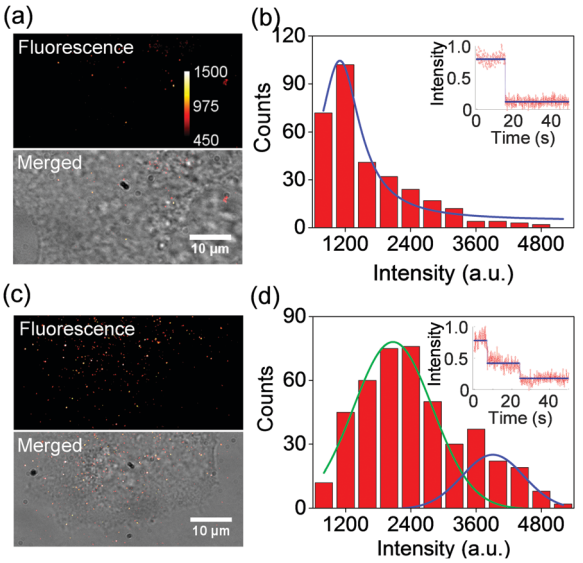


Fig. 3 Single-molecule fluorescence analysis of (a and b) N-Cy5-gA (0.1 nM) and (c and d) C-Cy5-gA (0.1 nM) in HepG2 cell membranes. (a and c) Representative fluorescence and bright field-fluorescence merged images; (b and d) the fluorescence intensity distribution of the fluorescent spots. Inset: The representative normalized photobleaching traces of the fluorescent spots with an intensity of (b) 1200 and (d) 2400.

To further investigate the channel structure in cell membranes, single-molecule fluorescence analysis was conducted (Section S5 in the ESI†).[15] For the experiments, gA was labeled with fluorescent dye Cy5 at its N- or C-terminus to afford N-Cy5-gA and C-Cy5-gA. The conductance values $\gamma_{\text{N-Cy5-gA}}$ (17.2 ± 0.6 pS) and $\gamma_{\text{C-Cy5-gA}}$ (22.8 ± 0.2 pS) were close to the above measured $\gamma_1$ and $\gamma_{gA}$ values, respectively (Fig. S11, ESI†). These correlations in $\gamma$ values clearly demonstrated that the structures of N-Cy5-gA and C-Cy5-gA in the bilayers should be the same as the structures of **1** and gA, respectively. After incubating HepG2 cells with N-Cy5-gA, red fluorescent spots were observed under microscopy (Fig. 3a). The spots with a fluorescence intensity arround 1200 showed the highest observed frequency (Fig. 3b). These spots exhibited characteristic one-step photobleaching traces (inset of Fig. 3b), indicating the recognition of one molecule of N-Cy5-gA from a single spot (with the observation frequency being 79%), whereas, under the same conditions, the positive control compound C-Cy5-gA was found to dimerize with the frequency being 73% (Fig. 3c and d), which is consistent with our expectation for the dimer structure of the gA peptide. All these findings clearly support that the channels from glycoside–gA conjugates in cell membranes should be unimolecular. The unimolecular structure of the conjugate is consistent with the above observation that the conjugate **1** has higher structural stability (higher $\tau_{1/2}$ value) than the supramolecular gA channel. This unimolecular structure is different from the expected double-stranded helix structure for deformylated gA,[12] probably due to steric hindrance from the N-terminus of the conjugate. Astonishingly, the unimolecular channel can result from the flexible structure of the bilayers that adapt to rigid and short helical structures (1.3 nm).[16]

The anticancer activities and cytotoxicity of **1–3** were then evaluated (Fig. 4a and Section S6 in the ESI†). Liver cancer cells (HepG2), human cervical cancer cells (HeLa), human pulmonary carcinoma cells (A549), human breast cancer cell lines (MCF-7), and healthy liver cells (LX-2) were used for evaluation. It was found that all the three conjugates showed anticancer activity toward the four cancer cells. Specifically, of the three conjugates, **1** exhibited the highest activity toward HepG2 cells with over-expressed ASGPR and relatively lower activity toward the other three cancer cells with a normal ASGPR level, which suggested its HepG2 cell-targeting behavior. Compared to **1**, conjugate **2** containing a longer spacer showed weak selectivity for HepG2 cells over the other three cancer cells, indicating that the longer spacer is not beneficial for targeting. Conjugate **3** displayed an unobservable preference for HepG2 cells. Considering that conjugate **1** is structurally different from **3** in the glycoside moiety, the above HepG2-targeting behavior of **1** can be rationally ascribed to the presence of Gal in its structure. Through pretreatment of HepG2 cells with Gal to block ASGPR, the cell viability in the presence of **1** obviously increased compared to the cells without Gal pretreatment (Fig. 4b), implying that the recognition of the Gal moiety of **1** to ASGPR promoted the targeting behavior.[17] Interestingly, in

 

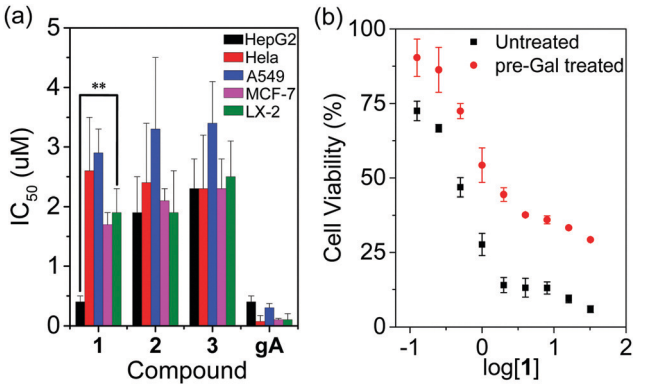


Fig. 4 (a) Anticancer activity of **1–3** and gA to liver cancer HepG2 cell (ASGPR overexpressed) and HeLa/A549/MCF-7 cell (normal ASGPR level), and their cytotoxicity to healthy liver LX-2 cells. Unpaired *t*-test analysis showed the existence of a significant difference between the $IC_{50}$ values of **1** toward HepG2 and other cells (**$P < 0.01$). (b) Dose-dependent HepG2 cell viability in the presence of **1**. The cells were with/without Gal pretreatment.

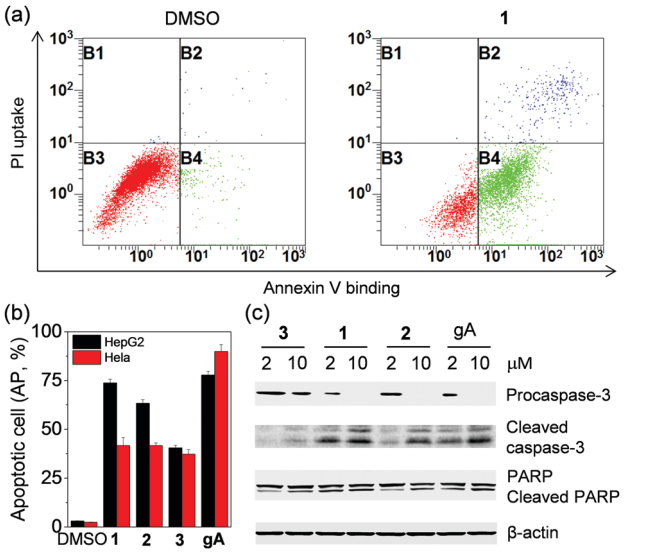


Fig. 5 (a) Flow cytometry analysis of the HepG2 cells treated with **1** (5.0 μM) for 48 h. (b) Apoptotic cell percentage (AP) of HepG2 and HeLa cells after treatment with conjugates **1–3** and gA for 48 h. (c) Immunoblotting of HepG2 cells treated with the peptides for 48 h.

contrast to gA, channel **1** showed obviously lower cytotoxicity to healthy liver LX-2 cells (Fig. 4a). The therapeutic window ($IC_{50}^{LX\text{-}2}/IC_{50}^{HepG2}$) of **1** was calculated to be 4.8, which is 24 times significantly higher than that of the primitive gA (0.2). Although this dose window is not high enough for therapeutic applications, the engineering strategy described here represents only the first attempt toward the goal. Moreover, conjugate **1** showed substantially lower hemolysis toxicity ($IC_{50}$ >60 μM) compared to that of gA ($IC_{50}$ = 7 μM) (Section S7 in the ESI,† and Fig. S14, ESI†), suggesting that the modification of gA at the N-terminus can lead to a significant decrease of the hemolysis toxicity of the peptide. However, similar to the primitive gA peptide, the conjugate with C-terminus modification showed obvious hemolysis toxicity. These results indicate that modification at the N-terminus of the gA peptide provided a new strategy to reduce the hemolysis toxicity of the peptide.

Cell death has been categorized into necrosis and apoptosis.[18] To identify the anticancer mechanism of **1–3**, flow cytometry analysis was performed (Section S8 in the ESI†). In the presence of the conjugates, both annexin $V^{pos}$–$PI^{neg}$ cells and annexin $V^{pos}$–$PI^{pos}$ cells were observed from the analysis (Fig. 5a and Fig. S15, ESI†), which were identified as the early and late stage apoptotic cells, respectively.[19] The observation of apoptotic cells demonstrated that the conjugates killed the cancer cells by inducing apoptosis. The apoptotic cell percentage (AP) was also determined (Fig. 5b). Significantly, **1** showed a higher $AP^{HepG2}/AP^{HeLa}$ ratio (1.8) than **3** (1.1) and primitive gA (0.8), further demonstrating that Gal-ASGPR recognition promoted the HepG2 cell-targeting behavior of **1**. Further analysis of the cell size showed obvious shrinkage after treatment of the cells with the conjugates (Fig. S16, ESI†). This finding ruled out cell death *via* the necrosis mechanism, as necrosis leads to cell swelling.[20]

Apoptotic cell death occurs mainly through caspase-dependent and independent mechanisms.[21] To identify the pathway of the apoptosis, western blot analysis was performed (Section S9 in the ESI†).[22] The results of immunoblotting of the peptide treated HepG2 cells showed that procaspase-3 was proteolytically cleaved to generate caspase-3 (Fig. 5c). Additionally, the endogenous caspase substrate, poly(ADP-ribose) polymerase (PARP), was also cleaved in the peptide treated cells. The observation of the cleaved caspase-3 and cleaved PARP demonstrated that the four peptides induced apoptotic cell death *via* a caspase-dependent pathway.[20] Importantly, for the HepG2 cells treated with **1**, the concentration of the cleaved caspase-3 was significantly higher than that of the cells treated with **3** (Fig. 5c). In contrast, a minimal difference was observed for HeLa cells treated with both peptides (Fig. S17, ESI†). This result provided further evidence that conjugate **1** exhibited liver cancer HepG2 cell-targeting behavior.

It has been established that perturbations in cellular ion concentrations caused by natural ion channels and synthetic ion transporters can lead to apoptosis of cancer cells.[20,22,23] To further verify the anticancer mechanism of the channels, the cellular ion transport was also investigated by assessing their ability to mediate cytosolic ion concentration changes (Section S10 in the ESI†). For the assessments, the ions' corresponding fluorescence probes were loaded into the cytoplasm by incubation with HepG2 cells. Compared to the cells without peptide treatment, the treatment of cells with the peptides could increase the cytosolic $H^+$ and $Na^+$ concentrations and reduce the cytosolic $K^+$ concentration (Fig. 6a–c). This finding is reasonable, because, for a live cancer cell, the cytosolic $H^+$ and $Na^+$ concentrations are lower than the extracellular fluid, whereas the $K^+$ concentration gradients are in a reverse direction.[24] Thus, inward $H^+$ and $Na^+$ flux and outward $K^+$ flux were observed.

It was also found that the incorporation of the conjugates into the cell membranes did not result in the variation of cytosolic $Ca^{2+}$ and $Cl^-$ concentrations (Fig. S18, ESI†). This is

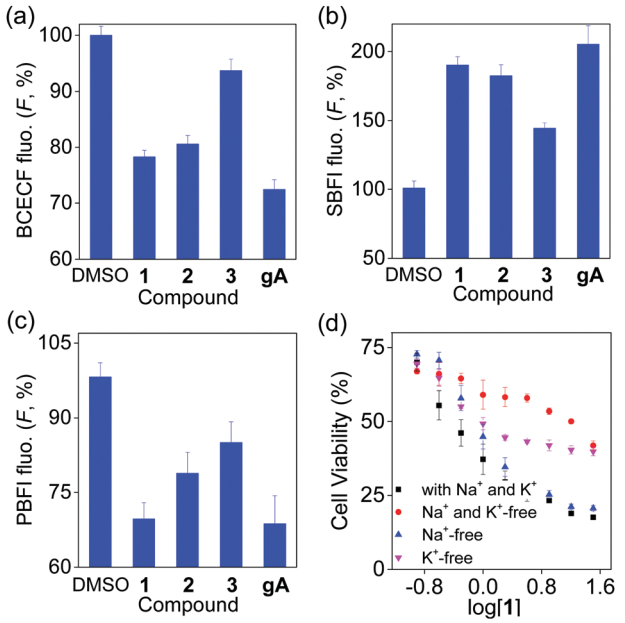


Fig. 6 Relative intracellular (a) BCECF ($H^+$ probe, its fluorescence intensity decreases with an increase in the $H^+$ concentration), (b) SBFI ($Na^+$ probe), and (c) PBFI ($K^+$ probe) fluorescence intensity after treatment of HepG2 cells with **1–3** and gA (5.0 μM) for 8 h. (d) Cell viability of HepG2 cells free of cytosolic $Na^+$ and/or $K^+$ after treatment with various concentrations of **1**.

expected because the channels based on the gA peptide can only mediate monovalent cation transport.[25] Importantly, the treatment of HepG2 cells free of $Na^+$ or $K^+$ with **1** led to a remarkable increase in the cell viability compared to the cells containing both ions (Fig. 6d). This result provided the first evidence that the channel-mediated ion transport induced apoptosis of the cells.

The time-dependent cellular ion transport demonstrated that cytosolic $H^+$, $Na^+$, and $K^+$ concentration variation occured shortly (<4 h) after the treatment of the cells with **1** (Fig. S19a, ESI†). The time-dependent flow cytometry experiments displayed an obvious increase in the annexin V-positive cell (apoptotic cell) percentage after treating the cells with **1** for 12 h (Fig. S19b, ESI†). These results suggested that apoptosis occurred after the ion transport. Thus, we can conclude that channel-mediated monovalent cation transport induced the apoptosis of the cancer cells.

In conclusion, we have prepared a compound with liver cancer cell-targeting behavior by engineering a gA peptide with galactose at the N-terminus. This conjugate forms unimolecular transmembrane channels in the cell membranes and enables the transport of monovalent cations to induce the apoptosis of cancer cells. The strategy described here for constructing a conjugate shows that it is possible to design molecules with increased cancer cell selectivity by changing the channel backbone and the binding moiety.[26]

This work was supported by the National Natural Science Foundation of China (NSFC) (Grant no. 21725202, 21921003, and 21971046), the National R&D Program of China (Grant no. 2017YFA0206901), and the Science and Technology Commission of Shanghai Municipality (Grant no. 18XD1400800 and 18JC1411600).

## Conflicts of interest

There are no conflicts to declare.

## Notes and references

1 R. J. Dubos, *J. Exp. Med.*, 1939, **70**, 1–10.
2 (*a*) D. W. Urry, *Proc. Natl. Acad. Sci. U. S. A.*, 1971, **68**, 672–676; (*b*) R. R. Ketchem, W. Hu and T. A. Cross, *Science*, 1993, **261**, 1457–1460.
3 O. S. Andersen, *Annu. Rev. Physiol.*, 1984, **46**, 531–548.
4 (*a*) J.-W. Liou, Y.-J. Hung, C.-H. Yang and Y.-C. Chen, *PLoS One*, 2015, **10**, e0117065; (*b*) W.-W. Haoyang, M. Zhang and J.-L. Hou, *Chin. J. Chem.*, 2019, **37**, 25–29.
5 (*a*) J. A. Killian, *Biochim. Biophys. Acta*, 1992, **1113**, 391–425; (*b*) D. A. Kelkar and A. Chattopadhyay, *Biochim. Biophys. Acta*, 2007, **1768**, 2011–2025; (*c*) F. Wang, L. Qin, C. J. Pace, P. Wong, R. Malonis and J. Gao, *ChemBioChem*, 2012, **13**, 51–55.
6 (*a*) C. J. Stankovic, S. H. Heinemann, J. M. Delfino, F. J. Sigworth and S. L. Schreiber, *Science*, 1989, **244**, 813–817; (*b*) D. J. Chadwick and G. Cardew, *Gramicidin and related ion channel-forming peptides*, Wiley, Chichester, 1999; (*c*) M. Mayer and J. Yang, *Acc. Chem. Res.*, 2013, **46**, 2998–3008; (*d*) P. Reiß and U. Koert, *Acc. Chem. Res.*, 2013, **46**, 2773–2780.
7 (*a*) T. I. Rokitskaya, Y. N. Antonenko and E. A. Kotova, *Biophys. J.*, 1997, **73**, 850–854; (*b*) V. L. Shapovalov, E. A. Kotova, T. I. Rokitskaya and Y. N. Antonenko, *Biophys. J.*, 1999, **77**, 299–305.
8 (*a*) D. Wijesinghe, M. C. M. Arachchige, A. Lu, Y. K. Reshetnyak and O. A. Andreev, *Sci. Rep.*, 2013, **3**, 3560; (*b*) J. M. David, T. A. Owens, L. J. Inge, R. M. Bremner and A. K. Rajasekaran, *Mol. Cancer Ther.*, 2014, **13**, 788–799; (*c*) J. M. David and A. K. Rajasekaran, *J. Kidney Cancer and VHL*, 2015, **2**, 15–24; (*d*) R.-Q. Wang, J. Geng, W.-J. Sheng, X.-J. Liu, M. Jiang and Y.-S. Zhen, *Cancer Cell Int.*, 2019, **19**, 145.
9 (*a*) G. Ashwell and J. Harford, *Annu. Rev. Biochem.*, 1982, **51**, 531–554; (*b*) M. Spiess, *Biochemistry*, 1990, **29**, 10009–10018.
10 A. A. D'Souza and P. V. Devarajan, *J. Controlled Release*, 2015, **203**, 126–139.
11 A. S. Arseniev, I. L. Barsukov, V. F. Bystrov, A. L. Lonize and Y. A. Ovchinikov, *FEBS Lett.*, 1985, **186**, 168–174.
12 S. M. Saparov, Y. N. Antonenko, R. E. Koeppe II and P. Pohl, *Biophys. J.*, 2000, **79**, 2526–2534.
13 A. Bandyopadhyay and J. Gao, Cancer-targeting peptides, in *Advances in the discovery and development of peptide therapeutics*, ed. G. Kruger and F. Albericio, Future Science Ltd, 2014.
14 (*a*) G. W. Gokel and A. Mukhopadhyay, *Chem. Soc. Rev.*, 2001, **30**, 274–286; (*b*) S. Matile, A. V. Jentzsch, J. Montenegro and A. Fin, *Chem. Soc. Rev.*, 2011, **40**, 2453–2474; (*c*) J. K. W. Chui and T. M. Fyles, *Chem. Soc. Rev.*, 2012, **41**, 148–175; (*d*) S.-P. Zheng, L.-B. Huang, Z. Sun and M. Barboiu, *Angew. Chem., Int. Ed.*, 2021, **60**, 566–597.
15 (*a*) H. Tan, Y. Huang, J. Xu, B. Chen, P. Zhang, Z. Ye, S. Liang, L. Xiao and Z. Liu, *Theranostics*, 2017, **7**, 3168–3178; (*b*) H. Tan, W. Luo, L. Wei, B. Chen, W. Li, L. Xiao, S. Manzhos, Z. Liu and S. Liang, *J. Phys. Chem. B*, 2016, **120**, 3081–3088.
16 O. V. Kondrashov, T. R. Galimzyanov, K. V. Pavlov, E. A. Kotova, Y. N. Antonenko and S. A. Akimov, *Biophys. J.*, 2018, **115**, 478–493.
17 X. Liu, W. Shao, Y. Zheng, C. Yao, L. Peng, D. Zhang, X.-Y. Hu and L. Wang, *Chem. Commun.*, 2017, **53**, 8596–8599.
18 V. Nikoletopoulou, M. Markaki, K. Palikaras and N. Tavernarakis, *Biochim. Biophys. Acta*, 2013, **1833**, 3448–3459.
19 J.-P. Aubry, A. Blaecke, S. Lecoanet-Henchoz, P. Jeannin, N. Herbault, G. Caron, V. Moine and J.-Y. Bonnefoy, *Cytometry*, 1999, **37**, 197–204.
20 (*a*) N. Busschaert, S.-H. Park, K.-H. Baek, Y. P. Choi, J. Park, E. N. W. Howe, J. R. Hiscock, L. E. Karagiannidis, I. Marques, V. Félix, W. Namkung, J. L. Sessler, P. A. Gale and I. Shin, *Nat. Chem.*, 2017, **9**, 667–675; (*b*) T. Saha, A. Gautam, A. Mukherjee, M. Lahiri and P. Talukdar, *J. Am. Chem. Soc.*, 2016, **138**, 16443–16451.
21 S. Elmore, *Toxicol. Pathol.*, 2007, **35**, 495–516.
22 F.-F. Shen, S.-Y. Dai, N.-K. Wong, S. Deng, A. S.-T. Wong and D. Yang, *J. Am. Chem. Soc.*, 2020, **142**, 10769–10779.
23 K. Kunzelmann, *Cell. Mol. Life Sci.*, 2016, **73**, 2387–2403.
24 S. O. Their, *Am. J. Med.*, 1986, **80**, 3–7.
25 V. B. Myers and D. A. Haydon, *Biochim. Biophys. Acta*, 1972, **274**, 313–322.
26 P. Teng, N. Ma, D. C. Cerrato, F. She, T. Odom, X. Wang, L.-J. Ming, A. Vaart, L. Wojtas, H. Xu and J. Cai, *J. Am. Chem. Soc.*, 2017, **139**, 7363–7369.

 